Synchronous Multi-Link Access in IEEE 802.11be: Modeling and Network Sum Rate Optimization

Jie Zhang*, Yayu Gao*, Xinghua Sun†, Wen Zhan†, Peng Liu‡ and Ziyang Guo‡
*School of Electronic Information and Communications, Huazhong University of Science and Technology
†School of Electronics and Communication Engineering, Sun Yat-sen University
‡Huawei Technologies Co., Ltd.
{jzhang_eic, yayugao}@hust.edu.cn, {sunxinghua, zhanw6}@mail.sysu.edu.cn, {jeremy.liupeng, guoziyang}@huawei.com

***Abstract*—Multi-link operation is considered to be one of the new key features in the next generation WiFi 7, i.e., IEEE 802.11be. This paper studies the maximum network sum rate of general M-link 802.11be networks with two different synchronous multi-link channel access methods being proposed by Task Group BE, i.e., Longest Backoff and Shortest Backoff. By using a Markov renewal process to model the behavior of each Head-of-Line packet, the explicit expressions of the maximum network sum rate and the corresponding optimal initial backoff window size are derived, and verified by simulation results. The analysis shows that Longest Backoff and Shortest Backoff achieve an identical maximum network sum rate. However, to achieve the performance limit, the initial backoff window sizes need to be adaptively tuned in a different manner under the two access methods. As the number of links grows, the initial backoff window size with Longest Backoff should be monotonically decreased, while that with Shortest Backoff should be enlarged.**

***Index Terms*—IEEE 802.11be, multi-link, random access, data rate optimization**

I. Introduction

Task Group BE (TGbe) is working on the next-generation IEEE 802.11be standard, also known as WiFi 7. Multi-link operation (MLO) [1] is considered as one of the revolutionary changes in 802.11be [2]. With MLO, a single device can transmit data on several links simultaneously, which is favorable for both extremely high data rate and low latency services. As multi-link devices (MLDs) may not be be able to support simultaneous transmission and reception (STR) due to in-device power leakage from insufficient frequency separation, the non-STR [3] mode with synchronous transmissions is being widely considered by TGbe, where various synchronous multi-link channel access methods have been proposed [4]–[7].

Simulation studies have validated that the newly-introduced MLO can significantly boost the data rate and latency performance [8]–[10]. By extending the classic Bianchi model [11], an analytical model for double-link IEEE 802.11be networks was proposed in [12]. The network sum rate performance can be numerically calculated by solving a set of non-linear equations. Due to the implicit nature of the solution, the performance limit, the maximum network sum rate, for instance, of multi-link IEEE 802.11be networks under different channel access methods still remains largely unknown.

In this paper, we provide closed-form solution to the above open question. We consider a synchronous multi-link IEEE 802.11be network with a general case of M links and two representative synchronous channel access methods: Longest Backoff and Shortest Backoff. In particular, by extending a unified analytical framework proposed for single-link IEEE 802.11 Distributed Coordination Function (DCF) networks [13] to incorporate synchronous multi-link channel access, the maximum network sum rate is derived as an explicit function of the number of links, the payload length, the slot length, the holding time in successful transmission and the holding time in collision. Analysis reveals that both Longest Backoff and Shortest Backoff achieve the same maximum network sum rate, which is proportional to the number of links.

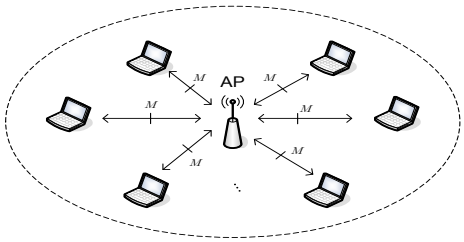

Fig. 1: Graphic illustration of an IEEE 802.11be network with multi-link devices

The optimal initial backoff window sizes under the two access methods are also obtained, and found to be increasing linearly with the number of MLDs. With Longest Backoff, the optimal initial backoff window size decreases as the number of links increases, however, with Shortest Backoff, it increases with the number of links. The analysis is verified by simulation results, which sheds important light on the design and optimization of the multi-link operation in the next-generation WiFi 7 networks.

The rest of the paper is organized as follows. Section II presents the system model and preliminary analysis. The network sum rate optimization is presented in Section III, and is verified by simulation results in Section IV. Finally, concluding remarks are summarized in Section V.

II. System Model and Preliminary Analysis

Consider an IEEE 802.11be network with n non-STR MLDs transmitting on M links as illustrated in Fig. 1. Assume that each link of an MLD performs the DCF protocol, and each MLD adopts identical backoff parameters, including the initial backoff window size W and the cutoff phase K. When an MLD accesses the channel, it will transmit a packet payload

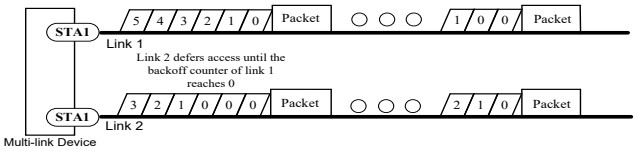

(a)

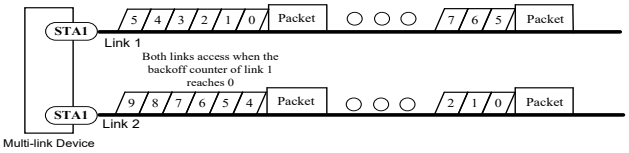

(b)

Fig. 2: Illustration of the two synchronous multi-link access methods. (a) Longest Backoff. (b) Shortest Backoff.

on each link. Each MLD has transmission rate R (in the unit of Mbps) on each link, and packet payload length L_P (in the unit of bits). As each link performs the backoff procedure independently, the backoff counters on different links are unlikely to reach zero simultaneously. To support synchronous channel access for each MLD, TGbe has been considering different types of access methods [4]–[7]. In this paper, we consider the following two representative channel access methods:

1) Longest Backoff (LB): An MLD makes a transmission request when the channel is idle, and the backoff counters on all the M links reach zero,
2) Shortest Backoff (SB): An MLD makes a transmission request when the channel is idle, and the backoff counters on any of the M links reaches zero,

which are illustrated in Fig. 2 respectively, for the case of $M = 2$. It can be seen that the classical single-link access adopted in IEEE 802.11 DCF can be regarded as a special case of $M = 1$.

A. Modeling: A Head-of-Line Packet Approach

In this paper, the analytical framework proposed in [13] for single-link IEEE 802.11 networks will be extended to model a multi-link IEEE 802.11be network. As we consider the synchronous channel access, the Head-of-Line (HOL) packets on different links within the same MLD will always be in the same state at any time. Therefore, we can focus on modeling the behavior of each HOL packet on one single link among the M links.

1) State Characterization of HOL Packets: First of all, a discrete-time Markov renewal process $(\boldsymbol{X}, \boldsymbol{V}) = \{(X_j, V_j), j = 0, 1, \ldots\}$ can be established to model the behavior of each HOL packet. X_j denotes the state of a tagged HOL packet at the jth transition and V_j denotes the epoch at which the jth transition occurs. Fig. 3 shows the embedded Markov chain $\boldsymbol{X} = \{X_j\}$.

Similar to [13], the states of X_j can be divided into three categories: 1) waiting to request (State $\mathrm{R}_i, i = 0, 1, \ldots, K$); 2) collision (State $\mathrm{F}_i, i = 0, 1, \ldots, K$); and 3) successful transmission (State T). Let $p^{(\phi)}$ denote the limiting probability of successful transmission of HOL packets given that the channel

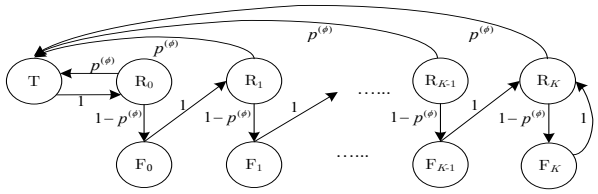

Fig. 3: Embedded Markov chain $\{X_j\}$ of the state transition process of an individual HOL packet in an MLD.

is idle, under the channel access method $\phi = LB, SB$. The steady-state probability distribution of the embedded Markov chain can be obtained as

$$\pi_{R_i}^{(\phi)} = \begin{cases} (1-p^{(\phi)})^i \pi_T^{(\phi)} & i = 0, 1, \ldots, K-1 \\ \frac{(1-p^{(\phi)})^K}{p^{(\phi)}} \pi_T^{(\phi)} & i = K \end{cases} \quad (1)$$

and

$$\pi_{F_i}^{(\phi)} = \pi_{R_i}^{(\phi)} \cdot (1 - p^{(\phi)}), \quad i = 0, 1, \ldots, K. \quad (2)$$

2) Holding time in States: The interval between successive transitions, i.e., $V_{j+1} - V_j$, is called the holding time in State X_j. In particular, the holding times in State T and State F_i are deterministic values which are determined by transmission parameters the MLDs choose, and the holding time in State R_i is stochastic, and closely dependent on the channel access method adopted by the MLDs. In the following, the holding times in State T, F_i and R_i will be derived.

Specifically, for a WiFi device, its holding time in successful transmission and collision, $\tau_T^{(LB)} = \tau_T^{(SB)} = \tau_T$ and $\tau_F^{(LB)} = \tau_F^{(SB)} = \tau_F$ (in the unit of time slots), can be written as

$$\tau_T = \big((L_P + \text{MAC header})/R + \text{SIFS} + \text{ACK/Basic rate} + \text{DIFS} + \text{PHY preamble}\big)/\sigma \quad (3)$$

and

$$\tau_F = \frac{(L_P + \text{MAC header})/R + \text{DIFS} + \text{PHY preamble}}{\sigma}, \quad (4)$$

respectively, where σ denotes the time slot length (in the unit of μs).

The mean holding time $\tau_{R_i}^{(\phi)}$ in State $\mathrm{R}_i, i = 0, 1, \ldots, K$, of an HOL packet, $\phi = LB, SB$, on the other hand, is closely dependent on the access method and backoff parameter. Similar to the single-link case, for an MLD with M links, HOL packets on each link of the MLD enter State R_i simultaneously, and each randomly selects a value from $\{0, \ldots, W_i - 1\}$ as its backoff counter, where W_i is the backoff window size, $i = 0, \ldots, K$, and counts down at each idle time slot. However, different from the single-link case, the HOL packet on one link may not leave Sate R_i when its own backoff counter reaches zero. Instead, the M HOL packets within the same MLD will leave State R_i simultaneously, and make transmission attempts when the *joint backoff counter* of the MLD reaches zero and the channel is idle. Here the *joint backoff counter* represents the actual number of idle slots the HOL packets need to wait before them can leave State R_i, and is closely dependent on the channel access method the MLD selects. Specifically, we have

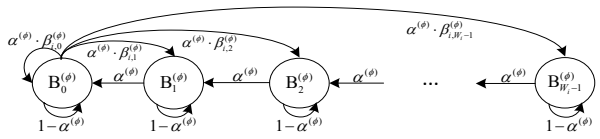

Fig. 4: State transition diagram of a State R_i HOL packet.

1) for $\phi = LB$, the *joint backoff counter* is the maximum value of the backoff counters on the M links;
2) for $\phi = SB$, the *joint backoff counter* is the minimum value of the backoff counters on the M links.

Let $G_t^{i,(\phi)}$ denote the state of the *joint backoff counter* of a State R_i HOL packet under the channel access method ϕ, at time slot t, $i = 0, \ldots, K$, $\phi = LB, SB$. The transition process of $\{G_t^{i,(\phi)}\}$ can be described by the Markov chain shown in Fig. 4, where $\alpha^{(\phi)}$ represents the probability of the channel being idle, $\beta_{i,j}^{(\phi)}$ represents the probability that the *joint backoff counter* is j when the HOL packet enters State R_i. As presented in Appendix A, the mean holding time $\tau_{R_i}^{(\phi)}$ in State R_i can be then obtained as

$$\tau_{R_i}^{(\phi)} = \frac{1}{\alpha^{(\phi)}} \cdot \sum_{j=0}^{W_i-1} (j+1)\, \beta_{i,j}^{(\phi)}, \tag{5}$$

$i = 1, \ldots, K, \phi = LB, SB$, where

$$\alpha^{(\phi)} = \frac{1}{1 + \tau_F - \tau_F p^{(\phi)} - (\tau_T - \tau_F) p^{(\phi)} \ln p^{(\phi)}}, \tag{6}$$

by following a similar derivation in [13].

With LB, the maximum value of the backoff counters is j means that all the backoff counters are less than or equal to j, while not all of them are less than j. Therefore, we have

$$\beta_{i,j}^{(LB)} = \left(\frac{j+1}{W_i}\right)^M - \left(\frac{j}{W_i}\right)^M. \tag{7}$$

Similarly, the minimum value of the backoff counters is j means that all the backoff counters are greater than or equal to j, while not all of them are greater than j, so $\beta_{i,j}^{(SB)}$ can be obtained as

$$\beta_{i,j}^{(SB)} = \left(\frac{W_i - j}{W_i}\right)^M - \left(\frac{W_i - (j+1)}{W_i}\right)^M. \tag{8}$$

By substituting (7) and (8) into (5), Appendix B shows that the mean holding time $\tau_{R_i}^{(LB)}$ and $\tau_{R_i}^{(SB)}$ can be further approximately obtained as

$$\tau_{R_i}^{(LB)} \approx \frac{1}{\alpha^{(LB)}} \cdot \left(\frac{MW_i}{M+1} + \frac{1}{2}\right) \tag{9}$$

and

$$\tau_{R_i}^{(SB)} \approx \frac{1}{\alpha^{(SB)}} \cdot \left(\frac{W_i}{M+1} + \frac{1}{2}\right), \tag{10}$$

respectively, when the initial backoff window size W is large enough and the number of links M is not too large.

3) Stationary State Probabilities: Finally, the limiting state probabilities of the Markov renewal process $(\boldsymbol{X}, \boldsymbol{V})$ are given by

$$\tilde{\pi}_j^{(\phi)} = \frac{\pi_j^{(\phi)} \tau_j^{(\phi)}}{\sum_{i \in Q} \pi_i^{(\phi)} \tau_i^{(\phi)}}, \tag{11}$$

where $\phi = LB, SB$, $j \in Q$, Q is the state space of $\boldsymbol{X}$.

B. Data Rate Performance

In a saturated network, for each link of an MLD, its link throughput $\lambda_{out}^{(\phi)}$, which is defined as the percentage of time used for successful transmission on the link, is equal to its service rate $\tilde{\pi}_T^{(\phi)}$, which can be written as

$$\lambda_{out}^{(LB)} = \tilde{\pi}_T^{(LB)} = \frac{(M+1)\alpha^{(LB)} p_A^{(LB)} (2p_A^{(LB)} - 1)\tau_T}{MW \cdot \left(p^{(LB)} - 2^K (1 - p^{(LB)})^{K+1}\right)}, \tag{12}$$

and

$$\lambda_{out}^{(SB)} = \tilde{\pi}_T^{(SB)} = \frac{(M+1)\alpha^{(SB)} p_A^{(SB)} (2p_A^{(SB)} - 1)\tau_T}{W \cdot \left(p^{(SB)} - 2^K (1 - p^{(SB)})^{K+1}\right)}, \tag{13}$$

respectively, by following a similar derivation in [14] , where $p_A^{(\phi)}, \phi = LB, SB$ is the network steady-state point, which is characterized as the non-zero root of the fixed-point equation of the steady-state probability of successful transmission of HOL packets given that the channel is idle, $p^{(\phi)}$:

$$p^{(LB)} = \exp\left\{\frac{-n(M+1)(2p^{(LB)} - 1)}{MW \cdot (p^{(LB)} - 2^K (1 - p^{(LB)})^{K+1})}\right\} \tag{14}$$

and

$$p^{(SB)} = \exp\left\{\frac{-n(M+1)(2p^{(SB)} - 1)}{W \cdot (p^{(SB)} - 2^K (1 - p^{(SB)})^{K+1})}\right\}, \tag{15}$$

respectively, by following a similar derivation in [13].

Note that the link throughput of each MLD evaluates how efficient the time is used for successful transmissions on each link. It, however, does not reflect how much information can be transmitted in terms of bits per second on all the M links. In this paper, we focus on the data rate, which is defined as the number of information bits that are successfully transmitted per second. For each MLD, its data rate $D^{(\phi)}, \phi = LB, SB$ is determined by 1) the link throughput $\lambda_{out}^{(\phi)}$, 2) the number of links M, 3) the fraction of time that is used for payload transmission in each successful transmission, and 4) the transmission rate R on each link, and can be written as

$$D^{(\phi)} = M\tilde{\pi}_T^{(\phi)} \cdot \frac{\frac{L_P}{\sigma R}}{\tau_T} \cdot R = M\tilde{\pi}_T^{(\phi)} \cdot \frac{L_P}{\sigma \tau_T}. \tag{16}$$

III. Network Sum Rate Optimization

In this section, we will study how to maximize the network sum rate by properly tuning the backoff parameters.

The network sum rate, which is the sum of data rate of all the MLDs, can be obtained as

$$\hat{D}^{(\phi)} = nD^{(\phi)} = \frac{-ML_P p_A^{(\phi)} \ln p_A^{(\phi)}}{\sigma\left(1 + \tau_F - \tau_F p_A^{(\phi)} - (\tau_T - \tau_F) p_A^{(\phi)} \ln p_A^{(\phi)}\right)}, \tag{17}$$

$\phi = LB, SB$, by combing (6) and (12)-(16).

By following a similar derivation in [14], the following theorem presents the maximum network sum rate $\hat{D}_{\max}$ and the corresponding optimal network steady-state point p_A^*.

Theorem 1. *The maximum network sum rate* $\hat{D}_{\max} = \max_{p_A^{(\phi)}} \hat{D}^{(\phi)}$ *is given by*

$$\hat{D}_{\max} = \frac{-ML_P \cdot \mathbb{W}_0\left(-\frac{1}{e(1+1/\tau_F)}\right)}{\sigma\left(\tau_F - (\tau_T - \tau_F)\mathbb{W}_0\left(-\frac{1}{e(1+1/\tau_F)}\right)\right)}, \quad (18)$$

which is achieved when

$$p_A^{(\phi)} = p_A^* = -(1+1/\tau_F)\mathbb{W}_0\left(-\frac{1}{e(1+1/\tau_F)}\right), \quad (19)$$

where $\mathbb{W}_0(\cdot)$ *is the principal branch of the Lambert W function [15].*

It is shown in Theorem 1 that the maximum network sum rate $\hat{D}_{\max}$ is independent to access methods, i.e., both access methods achieve the same maximum network sum rate. It is only determined by the number of links M, the payload length L_P, the slot length σ, the holding time in successful transmission τ_T and the holding time in collision τ_F. In this paper, we use the system parameters following IEEE 802.11ax standard [16], which are listed in Table I. In this case, the maximum network sum rate $\hat{D}_{\max}$ is given by

$$\hat{D}_{\max} = 95M \text{ Mbps}, \quad (20)$$

which is linear to the number of links M.

To achieve $\hat{D}_{\max}$, however, the backoff parameters should be carefully tuned such that $p_A^{(\phi)} = p_A^*$. By substituting (19) into (14) and (15), Corollary 1 presents the optimal initial backoff window size $W_m^{(\phi)}, \phi = LB, SB$, to achieve the maximum network sum rate $\hat{D}_{\max}$.

Corollary 1. *The optimal initial backoff window sizes* $W_m^{(LB)}$ *and* $W_m^{(SB)}$ *are given by*

$$W_m^{(LB)} = (\frac{1}{M} + 1) \cdot \frac{1 - 2p_A^*}{(p_A^* - 2^K(1-p_A^*)^{K+1})\ln p_A^*} \quad (21)$$

and

$$W_m^{(SB)} = (M+1)n \cdot \frac{1 - 2p_A^*}{(p_A^* - 2^K(1-p_A^*)^{K+1})\ln p_A^*}, \quad (22)$$

respectively.

We can clearly see from (21) and (22) that the optimal initial backoff window size $W_m^{(\phi)}$ is closely dependent on the number of MLDs n, number of links M and the access method ϕ. With the system parameters in Table I, we have

$$W_m^{(LB)} = 7.46n(\frac{1}{M} + 1) \quad (23)$$

and

$$W_m^{(SB)} = 7.46n(M+1), \quad (24)$$

respectively. For illustration, Fig. 5 plots the optimal initial backoff window size $W_m^{(\phi)}$ with both LB and SB. As we can see from Fig. 5, the optimal initial backoff window size linearly increases as network size n grows, which is similar to the single-link case. The increasing rate is dependent on the number of links, and varies with the channel access method the network chooses. In particular, with LB, $W_m^{(LB)}$ decreases as M increases, while with SB, $W_m^{(SB)}$ increases as M increases. As shown in Section II, the *joint backoff counter* of LB is the largest value of the M counters, so its average value increases with M grows. Therefore, an MLD with LB should decrease its initial backoff window size as the the number of links grows. In contrast, the *joint backoff counter* of SB is the smallest value of the M counters, so its average value decreases with M grows, leading to a growing $W_m^{(SB)}$ as M increases.

TABLE I: System Parameter Setting

Slot time σ	9 µs
PHY preamble	20 µs
SIFS	16 µs
DIFS	34 µs
ACK	112 bits
Payload length L_P	2^{17} bits
MAC header	288 bits
Channel bandwidth per link	20 MHz
Basic rate	24 Mbps
Transmission rate R	114.7 Mbps
Cutoff phase K	6

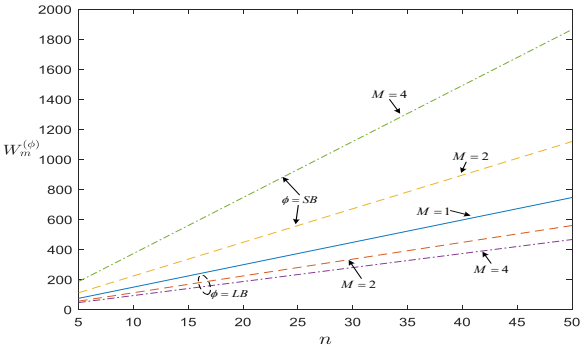

Fig. 5: Optimal initial backoff window size $W_m^{(\phi)}$ versus number of nodes n.

IV. Simulation Results

In this section, we will present the simulation results to verify the analysis presented in Section II and III. The system parameters used in the simulations are summarized in Table I.

Let us first consider the network sum rate performance of an IEEE 802.11be network with varied numbers of links and different channel access methods. The network sum rate $\hat{D}^{(\phi)}$ has been given in (17), which are verified by simulation results presented in Fig. 6. We can clearly see from Fig. 6 that the selection of initial backoff window size W is crucial to the network performance. The maximum network sum rate is identical for both LB and SB, and linearly increases as the number of links grows.

It can be further observed from Fig. 6 that the simulation results deviate from the analysis when the initial backoff window size W is small, which is more considerable for the case of SB with a larger number of links, $M = 4$, for instance. The reason is that under the saturated conditions, if the initial

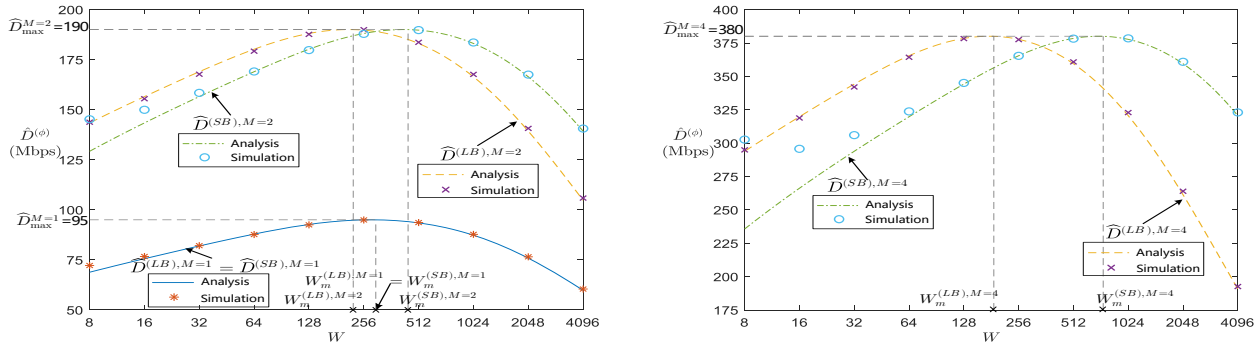

(a) (b)

Fig. 6: Network sum rate $\hat{D}^{(\phi)}$ versus the initial backoff window size W. $n = 20$. (a) $M = 1, 2$. (b) $M = 4$.

backoff window size is small, MLDs are often in deep backoff state with a large backoff window size. In this case, once an MLD makes a successful transmission, it will reset the backoff window size to the initial value W, and would likely to occupy the channel for several continuous transmissions, known as the "capture effect". In this case, the assumption that each MLD follows a time-homogeneous backoff process may not hold any more. As SB always selects the smallest value out of M backoff counters, the inaccuracy becomes more profound when M is large. If W is large enough, nevertheless, the transmission attempts can be randomized over the time. As Fig. 6b illustrates, with $W \geq 128$, the simulation results well agree with the analysis.

Fig. 7 presents how the network sum rate $\hat{D}^{(\phi)}$ varies with the number of nodes n. Corollary 1 in Section III shows that to achieve the maximum network sum rate, the initial backoff window size W should be carefully adjusted according to (21) and (22), respectively. As Fig. 7 shows, with a fixed initial backoff window size W, the network sum rate severely deteriorates with n when the network size is large due to the growing contention level. On the other hand, with the optimal initial backoff window size, the maximum network sum rate can be always achieved regardless of the variation of the network size.

V. Conclusions

In this paper, we address the network sum rate optimization of M-link IEEE 802.11be networks with two representative channel access methods, i.e., Longest Backoff and Shortest Backoff. Explicit expressions of maximum network sum rate and the corresponding optimal initial backoff window size are obtained. The analysis shows that both access methods can achieve the same maximum network sum rate, which is linear to the number of links M. To maximize the network sum rate, the initial backoff window size should be carefully tuned, which varies with the channel access method the network adopts. With Longest Backoff, the optimal initial backoff window size monotonically decreases as the number of links increases; while with Shortest Backoff, it increases with the number of links. The analysis provides direct guidance on the design and optimization of the multi-link operation introduced in future WiFi 7 networks.

Appendix A
Derivation of (5)

The Markov chain shown in Fig. 4 illustrates the transition process of $\{G_t^{i,(\phi)}\}$, where $G_t^{i,(\phi)}$ denotes the state of the *joint backoff counter* of a State-R$_i$ HOL packet at time slot t, $i = 0, \ldots, K, \phi = LB, SB$.

Let $Y_j^{(\phi)}$ denote the holding time of an HOL packet in State R$_i$. When an HOL packet enters State R$_i$, it randomly selects a number x from $\{0, \ldots, W_i - 1\}$ as the initial value of its *joint backoff counter*. According to Fig. 4, $Y_j^{(\phi)}$ is the sum of the sojourn time at states $\mathrm{B}_x^{(\phi)}, \mathrm{B}_{x-1}^{(\phi)}, \ldots, \mathrm{B}_0^{(\phi)}$, which can be written as

$$Y_j^{(\phi)} = \sum_{k=0}^{x} J_{B_k^{(\phi)}}, \tag{25}$$

where $J_{B_k^{(\phi)}}$ is the sojourn time at state $\mathrm{B}_k^{(\phi)}$, which follows a geometric distribution with parameter $\alpha^{(\phi)}$, and x follows a distribution that $\Pr\{x = j\} = \beta_{i,j}^{(\phi)}$. The mean holding time $\tau_{R_i}^{(\phi)}$ is then given by

$$\tau_{R_i}^{(\phi)} = \mathbb{E}[Y_j^{(\phi)}] = \frac{1}{\alpha^{(\phi)}} \cdot \sum_{j=0}^{W_i-1} (j+1)\, \beta_{i,j}^{(\phi)}. \tag{26}$$

Appendix B
Derivation of (9) and (10)

For LB, we have

$$\begin{aligned}\sum_{j=0}^{W_i-1} (j+1)\, \beta_{i,j}^{(LB)} &= \frac{1}{W_i^M} \cdot \sum_{j=0}^{W_i-1} \left((j+1)^M - j^M\right)(j+1) \\ &= \frac{1}{W_i^M} \cdot \left(\sum_{j=0}^{W_i-1} \left((j+1)^{M+1} - j^{M+1}\right) - \sum_{j=0}^{W_i-1} j^M \right) \\ &= \frac{1}{W_i^M} \cdot \left(W_i^{M+1} - \sum_{j=0}^{W_i-1} j^M \right). \end{aligned} \tag{27}$$

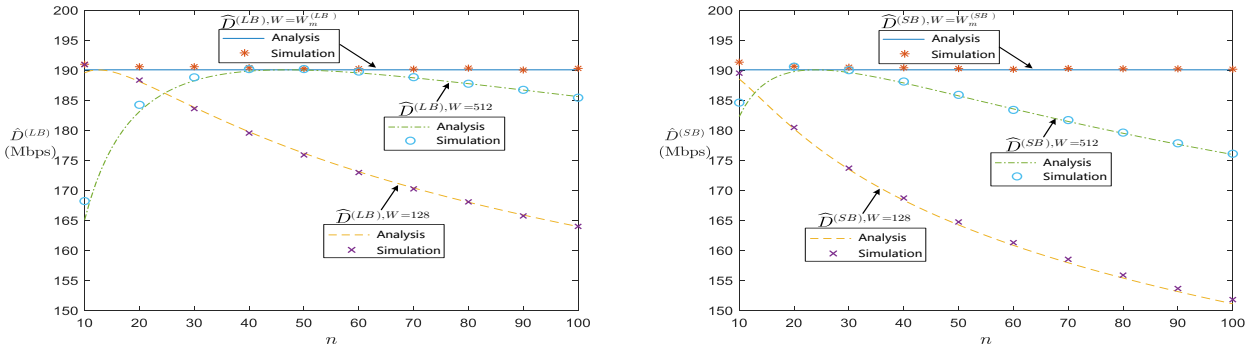

(a) (b)

Fig. 7: Network sum rate $\hat{D}^{(\phi)}$ versus the number of MLDs n. (a) LB. (b) SB.

We further have

$$\sum_{j=0}^{W_i-1} j^M = \frac{W_i^{M+1}}{M+1} - \frac{1}{2}W_i^M + \sum_{k=1}^{M} b_k W_i^{M-k}, \quad (28)$$

where $\{b_k, k = 1, \ldots, M\}$ are constants[1], by following Faulhaber's formula [17].

By substituting (28) to (27) , we have

$$\sum_{j=0}^{W_i-1}(j+1)\beta_{i,j}^{(LB)} = \frac{1}{W_i^M}\left(\frac{MW_i^{M+1}}{M+1} + \frac{1}{2}W_i^M - \sum_{k=1}^{M} b_k W_i^{M-k}\right)$$
$$= \frac{MW_i}{M+1} + \frac{1}{2} - \sum_{k=1}^{M} b_k W_i^{-k}. \quad (29)$$

For a large W and small M, the third term on the right of (29) is much smaller than the first and second terms, and can be ignored. We then have

$$\sum_{j=0}^{W_i-1} (j+1)\,\beta_{i,j}^{(LB)} \approx \frac{MW_i}{M+1} + \frac{1}{2}. \quad (30)$$

Similarly, for SB, we have

$$\sum_{j=0}^{W_i-1}(j+1)\beta_{i,j}^{S} = \frac{1}{W_i^M}\cdot\left(\sum_{j=0}^{W_i-1}\Big((W_i-j)^M j - \big(W_i-(j+1)\big)^M(j+1)\Big) + \sum_{j=0}^{W_i-1}(W_i-j)^M\right)$$
$$= \frac{1}{W_i^M}\cdot\sum_{j=0}^{W_i-1}(W_i-j)^M = \frac{1}{W_i^M}\cdot\sum_{j=1}^{W_i} j^M$$
$$\approx \frac{W_i}{M+1} + \frac{1}{2}. \quad (31)$$

REFERENCES

[1] A. Patil, G. Cherian, A. Asterjadhi, and D. Ho, "Multi-link operation: Design discussion," document IEEE 802.11-19/0823r2, Sep. 2019.

[2] E. Khorov, I. Levitsky, and I. F. Akyildiz, "Current status and directions of IEEE 802.11be, the future Wi-Fi 7," *IEEE Access*, vol. 8, pp. 88 664–88 688, May 2020.

[3] I. Jang, J. Choi, J. Kim, S. Kim, S. Park, and T. Song, "Considerations for multi-link channel access without simultaneous tx/rx capability," document IEEE 802.11-19/1917r1, Nov. 2019.

[4] ——, "Channel access for multi-link operation," document IEEE 802.11-19/1144r6, Nov. 2019.

[5] S. Naribole, S. Kandala, W. B. Lee, and A. Ranganath, "Multi-link channel access discussion," document IEEE 802.11-19/1405r7, Nov. 2019.

[6] Y. Seok, D. Akhmetov, D. Ho, R. Chitrakar, M. Gan, I. Jang, and S. Naribole, "UL sync channel access procedure," document IEEE 802.11-20/1730r3, Nov. 2020.

[7] Y. Li, Y. Guo, G. Huang, Y. Zhou, M. Gan, and D. Liang, "Channel access in multi-band operation," document IEEE 802.11-19/1116r5, Sep. 2019.

[8] S. Naribole, W. B. Lee, S. Kandala, and A. Ranganath, "Simultaneous transmit-receive multi-channel operation in next generation WLANs," in *Proc. IEEE WCNC*, 2020, pp. 1–8.

[9] G. Naik, D. Ogbe, and J. Park, "Can Wi-Fi 7 support real-time applications? on the impact of multi link aggregation on latency," in *Proc. IEEE ICC*, 2021, pp. 1–6.

[10] S. Naribole, S. Kandala, and A. Ranganath, "Multi-channel mobile access point in next-generation IEEE 802.11be WLANs," in *Proc. IEEE ICC*, 2021, pp. 1–7.

[11] G. Bianchi, "Performance analysis of the IEEE 802.11 distributed coordination function," *IEEE J. Sel. Areas Commun.*, vol. 18, no. 3, pp. 535–547, Mar. 2000.

[12] T. Song and T. Kim, "Performance analysis of synchronous multi-radio multi-link MAC protocols in IEEE 802.11be extremely high throughput WLANs," *Appl. Sci.*, vol. 11, no. 1, Dec. 2021.

[13] L. Dai and X. Sun, "A unified analysis of IEEE 802.11 DCF networks: Stability, throughput, and delay," *IEEE Trans. Mobile Comput.*, vol. 12, no. 8, pp. 1558–1572, Aug. 2013.

[14] Y. Gao, X. Sun, and L. Dai, "Throughput optimization of heterogeneous IEEE 802.11 DCF networks," *IEEE Trans. Wireless Commun.*, Jan. 2013.

[15] R. M. Corless, G. H. Gonnet, D. E. G. Hare, D. J. Jeffrey, and D. E. Knuth, "On the Lambert W function," *Adv. Comput. Math.*, Dec. 1996.

[16] *IEEE Standard for Information Technology–Telecommunications and Information Exchange between Systems Local and Metropolitan Area Networks–Specific Requirements Part 11: Wireless LAN Medium Access Control (MAC) and Physical Layer (PHY) Specifications Amendment 1: Enhancements for High-Efficiency WLAN*, IEEE Std 802.11ax-2021 (Amendment to IEEE Std 802.11-2020), 2021.

[17] D. E. Knuth, "Johann Faulhaber and sums of powers," *Math. Comput.*, vol. 61, pp. 277–294, July 1993.

[1]The detailed values of $\{b_k, k = 1, \ldots, M\}$ can be found on http://122.205.5.5:8084/~yayugao/students/jie_zhang/jie_zhang.html, which are omitted here due to limited space